Impact of Hybrid Nanoparticles (Au, Cu/Blood-Mediated) Transport in Stenotic and Aneurysmal Curved Artery with Gyrotactic Microorganism: Hematocrit-Based Viscosity Framework

Sarowa Sumit*, Kumar Surendra and Yadav Yashasvi
University Institute of Engineering and Technology, Maharshi Dayanand University, Rohtak, Haryana, INDIA
*sumitsarowa@gmail.com

Abstract

This study investigates the hemodynamic disturbances caused by stenosis and aneurysms in a curved artery, focusing on the innovative application of hybrid nanoparticles, specifically gold and copper. A mathematical model is characterized as an unsteady blood flow through a porous medium. The Forward Time Central Space scheme is used to solve resulting equations, to examine blood flow dynamics. This investigation aims to analyze the blood flow behavior due to hybrid nanoparticles in an artery subjected to an external magnetic field and to assess their impact on heat and mass transfer.

The results acquired for velocity, temperature, concentration, microorganism, wall shear stress and flow rate are displayed graphically and analyzed for several physical characteristics like Schmidt parameter, chemical reaction parameter, Grashoff number, radiation parameter and Reynolds number. This comprehensive evaluation offers insights into the complex interplay of fluid dynamics, flow behavior due to nanoparticles and biological factors in the context of cardiovascular well-being. It is observed that hybrid nanoparticles have the potential to regulate blood velocity and temperature, allowing Surgeons to make necessary adjustments as needed.

Keywords: Magnetohydrodynamics, Stenosis, Aneurysm, Hybrid nanoparticle, Heat and mass transfer.

Introduction

Nowadays, cardiovascular diseases are the prominent causes of morbidity and mortality worldwide, accounting for more than 50% of fatalities [7]. Cardiovascular disease includes high blood pressure, heart failure and various cardiac disorders such as stenosis and aneurysm. Stenosis (atherosclerosis) refers to the abnormal narrowing of the arterial channels, which is usually caused by plaque deposition, accumulation of fatty substances and irregular intra-vascular growth. Cholesterol, mainly low-density lipoprotein, plays a significant role in the progression of atherosclerosis[6,8]. In contrast, the aneurysm is identified by an abnormal dilation of arterial walls, usually resulting from weakened vessel structures. These dilations disrupt the flow dynamics, creating zones of low shear stress and recirculation that can encourage clot formation or, in extreme cases, vessel rupture.

Kawaguti and Hamano[11] investigated post-stenotic dilation through a numerical approach. In their study, they found that narrowing due to stenosis causes an increase in pressure and decreases the supply of oxygen to tissues. Moayeri and Zendehbudi[16] examined the influence of wall elasticity on blood flow attributes via the stenosed artery. Changdar and De[5] investigated the phenomenon of pulsatile blood flow in diseased artery that include multiple stenosis by utilizing numerical simulation. Tripathi and Sharma[31] described a mathematical framework that elaborates on the impact of varying viscosity through arterial stenosis.

The impact of multiple stenosis and aneurysm in the artery considering blood as Casson fluid was examined by Pincombe et al.[18] Theoretical modeling of dynamics of blood through coronary arteries along with a number of aneurysms and stenosis was done by Wong et al.[32] To understand the realistic behavior of blood flow, it becomes crucial to study flow behavior in curved artery. The nano-Eyring-Powell of blood via curved artery exhibiting time-varying atherosclerosis and aneurysm was numerically simulated by Sultan et al.[27] Various fluid flow interactions using experimental and simulation methodologies were studied revealing an increase in Reynolds number leading to a rise in the formation of vortices, along with an increase in both velocity and tension within the aneurysm.

Magnetic radiation affects the plasma contained in the blood. Kolin[12] studied magnetic field radiation effect in blood flow. Tripathi et al[30] explored heat and mass transfer influence on magneto-hydrodynamic in core and plasma region. In their investigation, they found that as the intensity of magnetic field and radiation parameter increases, there is a corresponding decrease in both temperature and velocity profiles. Imoro et al[9] studied magneto-hydrodynamic influence on flow of blood-based hybrid nanofluid in arterial stenosis, taking into accounts the effect of thermal radiation.

Due to their unique physical and chemical properties, nanoparticles offer promising potential for enhancing the treatment of cardiovascular diseases. They can serve as contrast agents in imaging techniques or as carriers for targeted drug delivery. The metal-based nanoparticles influence on blood flow via stenosed arteries with porous walls is theoretically analyzed by Nadeem and Ijaz[17].

Sharma et al[21] studied hematocrit-dependent viscosity technique for computational biomedical simulations regarding the transport of hybrid nanoparticles in a stenosed and aneurysmal curved artery, acknowledging the phenomenon of heat and mass transfer.

Heat and mass transfer are fundamental to comprehending the hemodynamics, especially in stenosed arteries where the flow is restricted. Kandasamy et al[10] studied the effect of transportation of heat and mass transfer under influence of magnetic field via stretched surface. The MHD effect on two-layered blood flow was also studied taking into account heat and mass transfer.[13]

It was found that a rise in radiation parameter decrease the velocity of blood flow. Sharma et al[21] evaluated the Nusselt number as heat transfer rate and Sherwood number as mass transfer rate along with activation energy effect on magnetohydrodynamic stretching surface. Mishra[15] explored the influence of heat and mass transfer on nanofluid flow through a slanted stenosed artery.

The study of microorganisms in blood flow is a pivotal field in biomedicine and biofluid dynamics, as it deals with how microorganisms (like bacteria, viruses, or engineered micro/nanoparticles) interact with the bloodstream under various physiological and pathological conditions. A numerical assessment to evaluate the effect of radiation and magnetic intensity with microorganisms in the flow across vertical and curved sheet was implemented by Anantha et al[3].

Alharbi et al[2] carried out bioconvection micro-organisms correlated to hybrid nanofluid undergoing laminar incompressible flow in conjunction with nanoparticles and chemical reaction as a medium for targeted drug delivery.

Sharma et al[22] examined study of entropy generation in a ternary hybrid-nanofluid with gyrotactic microorganism situated in a bifurcated artery. Shit et al[25] used the Frobenius technique to describe the flow of blood via a tapering, stenotic artery accompanied by hematocrit-dependent viscosity.

The present study addresses a mathematical model that considers the impacts of hybrid gold-copper nanoparticles, magnetic fields and microorganism interactions to examine blood flow dynamics in a curved artery impacted by stenosis and aneurysms. The following are the aims of the current investigation:

1. Analyze the hemodynamic disturbances induced by stenosis and aneurysms in a curved artery.
2. Explore the distribution and flow behavior due to hybrid nanoparticles (Gold and Copper) in diseased artery under the effect of an external magnetic field.
3. Assess the interaction between microorganisms and electrical conductivity in blood flow.
4. Analyze the impact due to hybrid nanofluid (Au, Cu/blood) on Wall Shear Stress, Nusselt number, Sherwood Number and flow rate.

Integrating these factors into a single model, this work provides a comprehensive perspective for acknowledging the complex interplay of biological, chemical and physical phenomena in diseased arteries. The findings aim to contribute to advancements in cardiovascular diagnostics, nanoparticle-based therapies and the acknowledgment of magnetohydrodynamics in medical research.

Material and Methods

In this investigation, cardiovascular diseases stenosis and aneurysm are both studied simultaneously in an artery, considering blood as Newtonian in nature. To understand realistic behavior of the artery, we took the artery in curved shape. The $r-$ axis and x−axis are symbolized as radial and axial direction respectively. Hematocrit-dependent variable viscosity is utilized. This model is characterized by an unsteady blood flow through a porous medium. The blood is concentrated by plasma, which is affected by magnetic field subjected uniformly in axial direction. Gold and copper nanoparticles are injected into blood to get hybrid nanofluid as portrayed in fig. 1.

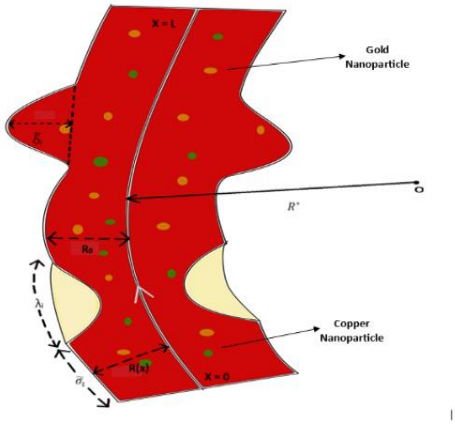

Fig. 1: Geometric diseased artery

Geometry of stenosis and aneurysm diseased artery can be determined as follows[24,28]:

$$R(x) = \begin{cases} (R_0 + \tilde{a}_i\, x)\left(1 - \left(\frac{\tilde{\delta}_i}{2R_0}\left(1 + cos\frac{2\pi}{\lambda_i}\left(x - \tilde{\sigma}_i - \frac{\lambda_i}{2}\right)\right)\right)\right) \\ , \ \tilde{\sigma}_i \le x \le \tilde{\sigma}_i + \lambda_i, i = 1,2 \\ (\tilde{a}_i x + R_0), \ Otherwise, \end{cases}.$$

$$-R(x) = \begin{cases} (\tilde{a}_i x - R_0)\left(1 - \left(\frac{\tilde{\delta}_i}{2R_0}\left(1 + cos\frac{2\pi}{\lambda_i}\left(x - \tilde{\sigma}_i - \frac{\lambda_i}{2}\right)\right)\right)\right) \\ \tilde{\sigma}_i \le x \le \tilde{\sigma}_i + \lambda_i, i = 1,2 \\ (\tilde{a}_i x - R_0), \ Otherwise, \end{cases} \quad (1)$$

The geometry of upper and lower wall of the curved-artery is represented as $R(x)$ and $-R(x)$ respectively. L is taken as arterial length. $a = tan(\varphi)$ is referred to as the tapered parameter and φ is the tapering angle in equation. λ_i is denoted as length of diseased segment, $\tilde{\sigma}_i$ is length of i^{th} abnormal region from origin and $\tilde{\delta}_i$ represents critical height of i^{th} diseased section taking place at explicit points specified through: $x = \widetilde{\sigma_1} + \frac{\lambda_i}{2}$ and $x = \widetilde{\sigma_2} + \frac{\lambda_i}{2}$, although value of $\tilde{\delta}_i$ is positive for stenosis and for aneurysm, it is negative.

Governing equations of continuity, momentum in radial and axial, temperature, concentration and microorganism equations in dimensional form are taken as follows:[9,20,22]

$$\frac{\partial u_1}{\partial r} + \frac{u_1}{R^*+r} + \frac{R^*}{R^*+r}\left(\frac{\partial v_1}{\partial r}\right) = 0. \tag{2}$$

$$\rho_{hnf}\left[\frac{\partial u_1}{\partial t} + u_1\frac{\partial u_1}{\partial r} + \frac{R^* v_1}{R^*+r}\frac{\partial v_1}{\partial x} - \frac{{v_1}^2}{R^*+r}\right] = -\frac{\partial P}{\partial r} + \mu_{hnf}\left[\frac{\partial^2 u_1}{\partial r^2} + \frac{1}{R^*+r}\frac{\partial u_1}{\partial r} + \left(\frac{R^*}{R^*+r}\right)^2\frac{\partial^2 u_1}{\partial x^2} - \frac{u_1}{(R^*+r)^2} - \frac{2R^*}{(R^*+r)^2}\frac{\partial v_1}{\partial x}\right] + \left(\frac{4}{3}\frac{\partial u_1}{\partial r} - \frac{2}{3}\left(\frac{R^*}{R^*+r}\frac{\partial v_1}{\partial x} + \frac{u_1}{R^*+r}\right)\right)\frac{\partial \mu_{hnf}}{\partial r}. \tag{3}$$

$$\rho_{hnf}\left[\frac{\partial v_1}{\partial t} + v_1\frac{\partial v_1}{\partial r} + \frac{R^* v_1}{R^*+r}\frac{\partial v_1}{\partial x} - \frac{u_1 v_1}{R^*+r}\right] = -\frac{R^*}{R^*+r}\frac{\partial P}{\partial x} + G(t) + \mu_{hnf}\left[\frac{\partial^2 v_1}{\partial r^2} + \frac{1}{R^*+r}\frac{\partial v_1}{\partial r} + \left(\frac{R^*}{R^*+r}\right)^2\frac{\partial^2 v_1}{\partial x^2} - \frac{v_1}{(R^*+r)^2} - \frac{2R^*}{(R^*+r)^2}\frac{\partial u_1}{\partial x}\right] + \left(\frac{R^*}{R^*+r}\frac{\partial u_1}{\partial x} + \frac{\partial v_1}{\partial r} - \frac{v_1}{R^*+r}\right)\frac{\partial \mu_{hnf}}{\partial r} - \sigma_{hnf}B^2 v_1 - \frac{\mu_{hnf}}{K}v_1. + g(\rho\beta)_{hnf}(T - T_W) + g(\rho\beta)_{hnf}(C - C_W). \tag{4}$$

$$(\rho C_P)_{hnf}\left[\frac{\partial T_1}{\partial t} + u_1\frac{\partial T_1}{\partial r} + \frac{R^*}{R^*+r}\frac{\partial T_1}{\partial x}\right] = K_{hnf}\left[\frac{\partial^2 T_1}{\partial r^2} + \frac{1}{R^*+r}\frac{\partial T_1}{\partial r} + \left(\frac{R^*}{R^*+r}\right)^2\frac{\partial^2 T_1}{\partial x^2}\right] - \frac{\partial q}{\partial r}. \tag{5}$$

$$\left[\frac{\partial C_1}{\partial t} + u_1\frac{\partial C_1}{\partial r} + \frac{R^*}{R^*+r}\frac{\partial C_1}{\partial x}\right] = D_m\left[\frac{\partial^2 C_1}{\partial r^2} + \frac{1}{R^*+r}\frac{\partial C_1}{\partial r} + \left(\frac{R^*}{R^*+r}\right)^2\frac{\partial^2 C_1}{\partial x^2}\right] - R_b(C - C_W). \tag{6}$$

$$\left[\frac{\partial n_1}{\partial t} + u_1\frac{\partial n_1}{\partial r} + \frac{R^* n_1}{R^*+r}\frac{\partial n_1}{\partial x}\right] + \frac{bW_c}{C_0 - C_W}\left[\frac{\partial}{\partial r}\left(\frac{n_1\partial C_1}{\partial r} + \frac{\partial}{\partial x}\left(\frac{n_1\partial C_1}{\partial x}\right)\right)\right] = D_n\left[\frac{\partial^2 n_1}{\partial r^2} + \frac{1}{R^*+r}\frac{\partial n_1}{\partial r} + \left(\frac{R^*}{R^*+r}\right)^2\frac{\partial^2 n_1}{\partial x^2}\right]. \tag{7}$$

The below mentioned equality defines the mathematical presentation for the axial pressure gradient:

$$-\frac{\partial P}{\partial x} = P_0 + P_1 cos(2\pi\omega_P t), \quad t > 0. \tag{8}$$

where P_0 = Mean pressure gradient, $\omega_P = 2\pi f_p$.

P_1 = Magnitude of pulsatile component that sustains both the diastolic and systolic pressure.

The external periodic body acceleration imparted in axial direction of the hybrid nanofluid is expressed by utilizing following equation:

$G(t) = \overline{P_0} cos(\overline{\omega_2}t + \chi)$, $t > 0$, where χ is the phase angle and $\overline{\omega_2} = 2\pi f_p$.

Initial and boundary conditions for the flow equations are as follows:

$$\left\{\begin{array}{c} v_1 = T = C = n_1 = 0 \; at \; t = 0, \\ \overline{v_1} = 0, \; C = C_W, \; T = T_W, n_1 = n_w \\ at \; r = R \; and \; r = -R \end{array}\right\} \tag{9}$$

The mathematical interpretation for hematocrit dependent viscosity is defined as [19]:

$$\mu_f = \mu_0[1 + \beta_1 h(r)]. \tag{10}$$

From above, $h(r) = h_m\left[1 - \left(\frac{r}{R_0}\right)^m\right]$, h_m = maximum hematocrit at the mid-point of artery, β_1 =2.5, m stands for flow shape i.e. m is greater than or equal to 2. The expression of thermo-physical parameters of hybrid nanofluids taken into this analysis, are enumerated in the table 2.

Non-dimensional form of governing equations: To get a numerical solution, the governing equations must be transformed into dimensionless form. The following parameters are acquainted to non-dimensionalized governing relationship:

$$r = \frac{r}{R_0}, x = \frac{x}{\lambda_i}, \overline{u_1} = \frac{\lambda_i u_1}{\tilde{\delta} u_0}, \overline{v_1} = \frac{v_1}{u_0}, \bar{t} = \frac{u_0 t}{R_0}, R_c = \frac{R^*}{R_0}, \bar{P} = \frac{R_0^2 P}{\mu_0 u_0 \lambda_i}, Re = \frac{\rho_f u_0 R_0}{\mu_0}, \delta = \frac{\tilde{\delta}_i}{R_0}, \theta = \frac{T - T_0}{T_W - T_0}, \phi = \frac{C - C_0}{C_W - C_0}, Gr = \frac{g(\rho\beta)_f R_0^2 T_W}{\mu_0 u_0}, Gm = \frac{g(\rho\beta)_f R_0^2 C_W}{\mu_0 u_0}, M^2 = \frac{\sigma_f B^2 R_0^2}{\mu_0}, \xi = \frac{R_b \rho_f R_0^2}{\mu_0}, Sc = \frac{v_1}{D_m}, Pr = \frac{\mu_0 (C_P)_f}{K_f}, Nr = \frac{16\sigma_e T_c^3}{\beta_r K_f}, \in = \frac{R_0}{\lambda_i}, Z = \frac{K}{R_0^2}, \bar{\chi} = \frac{n - n_1}{n_w - n_1}, Sb = \frac{v_1}{D_n}, Pe = \frac{bW_c}{D_n}, \sigma = \frac{n}{n_w - n_1}.$$

Using mild-stenosis case i.e. $\delta\left(= \frac{\tilde{\delta}_i}{R_0}\right) << 1$, $\in \left(= \frac{R_0}{\lambda_i}\right) = O(1)$ and dimensionless parameters, equations are to be reduce in dimensionless form.

Currently, the curved arterial channel's non-dimensionalized shape with stenosis and aneurysm is mentioned below:

$$R(x) = \left\{\begin{array}{c} (ax+1)\left(1 - \left(\frac{\delta}{2}\left(1 + cos2\pi\left(x - \sigma_i - \frac{1}{2}\right)\right)\right)\right) \\ , \; \sigma_i \le x \le \sigma_i + 1, i = 1, 2 \\ (ax+1) \; Otherwise, \end{array}\right\}.$$

$$-R(x) = \left\{\begin{array}{c} (1+ax)\left(1 - \left(\frac{\delta}{2}\left(1 + cos2\pi\left(x - \sigma_i - \frac{1}{2}\right)\right)\right)\right) \\ , \; \sigma_i \le x \le \sigma_i + 1, i = 1, 2 \\ (1-ax) \; Otherwise, \end{array}\right\} \tag{11}$$

Here, $\sigma_i = \frac{\tilde{\sigma}_i}{\lambda_i}$; $\alpha = \frac{\tilde{a}_i \lambda_i}{R_0}$.
$\alpha = tan(\varphi)$ is referred to as the tapering parameter and φ is related taper angle in equation. The curved channel's non-

tapered, convergent and divergent tapering were denoted by the conditions $\varphi = 0$, $\varphi > 0$ and $\varphi < 0$ respectively.

Governing formulae in dimensionless form after applying non-dimensional factors on governing equations are as follows:

$$\frac{\partial \bar{P}}{\partial r} = 0. \tag{12}$$

$$\frac{\rho_{hnf}}{\rho_f} Re \frac{\partial \overline{v_1}}{\partial \bar{t}} = -\frac{R_c}{R_c+\bar{r}} \frac{\partial \bar{P}}{\partial \bar{x}} + G(\bar{t}) + \frac{\mu_{hnf}}{\mu_0} \left[\frac{\partial^2 v_1}{\partial \bar{r}^2} + \frac{1}{R_c+\bar{r}} \frac{\partial \overline{v_1}}{\partial \bar{r}} + -\frac{\overline{v_1}}{(R_c+\bar{r})^2} \right] - \left(\frac{\partial \overline{v_1}}{\partial \bar{r}} - \frac{\overline{v_1}}{R_c+\bar{r}} \right) \frac{m\beta_1 h_m \bar{r}^{m-1}}{(1-\phi_1)^{2.5}(1-\phi_2)^{2.5}} - \frac{\sigma_{hnf}}{\sigma_f} M^2 \overline{v_1} - \frac{\mu_{hnf}}{\mu_0} \frac{\overline{v_1}}{Z} + \frac{(\rho\beta)_{hnf}}{(\rho\beta)_f} (Gr\theta + Gm\phi). \tag{13}$$

$$\frac{(\rho C_P)_{hnf}}{(\rho C_P)_f} \frac{K_f}{K_{hnf}} PrRe \frac{\partial \theta}{\partial \bar{t}} = \frac{\partial^2 \theta}{\partial \bar{r}^2} + \frac{1}{R_c+\bar{r}} \frac{\partial \theta}{\partial \bar{r}} + \frac{\partial^2 T_1}{\partial x^2} - \frac{K_f}{K_{hnf}} Nr \frac{\partial^2 \theta}{\partial \bar{r}^2}. \tag{14}$$

$$ReSc \frac{\partial \phi}{\partial \bar{t}} = \frac{\partial^2 \phi}{\partial \bar{r}^2} + \frac{1}{R_c+\bar{r}} \frac{\partial \phi}{\partial \bar{r}} - Sc\xi\phi. \tag{15}$$

$$ReSb \frac{\partial \bar{\chi}}{\partial \bar{t}} = \frac{\partial^2 \bar{\chi}}{\partial \bar{r}^2} + \frac{1}{R_c+\bar{r}} \frac{\partial \bar{\chi}}{\partial \bar{r}} - Pe\sigma \left(\frac{\partial \bar{\chi}}{\partial \bar{r}} \frac{\partial \phi}{\partial \bar{r}} + (\sigma + \bar{\chi}) \frac{\partial^2 \phi}{\partial \bar{r}^2} \right) \tag{16}$$

The accompanying initial and boundary conditions that are subject to the flow, are transformed in the non-dimensionalized form as follows:

$$\left\{ \begin{matrix} \overline{v_1} = \theta = \phi = \bar{\chi} = 0 \; at \; t = 0, \\ \overline{v_1} = 0, \; = \phi = \bar{\chi} = 1 \; at \; r = R \; and \; r = -R \end{matrix} \right\}. \tag{17}$$

Now, by non-dimensionalization of Nusselt number (Nu), Sherwood number (Sh) and wall shear-stress (WSS) using non-dimensional parameters, we get:

$$Nu = -Re_x{}^{1/2} \frac{\partial \theta}{\partial x}, Sh = -Re_x{}^{1/2} \frac{\partial \phi}{\partial x}, WSS = -Re_x{}^{1/2} \frac{\partial v_1}{\partial x}.$$

Solution Process: Analytical solutions to the governing non-linear equations are difficult since they are coupled partial difference equations. So, numerical technique Forward Time Central Space (FTCS) methodology on MATLAB is used to solve equations (12)-(16) for the existing blood flow model. The suitable mesh size to aforementioned problem is $dx = 0.025$. Using above said scheme, the partial spatial and temporal derivatives are expressed as follows:

$$\frac{\partial \overline{v_1}}{\partial \bar{r}} = \frac{v_1(i+1,j) - v_1(i-1,j)}{2d\bar{r}}, \quad \frac{\partial^2 \overline{v_1}}{\partial \bar{r}^2} = \frac{v_1(i+1,j) - 2v_1(i,j) + v_1(i-1,j)}{d\bar{r}^2},$$
$$\frac{\partial \overline{v_1}}{\partial \bar{t}} = \frac{v_1(i,j+1) - v_1(i,j)}{dt}.$$

Validation of the results: Our study's validation is completed by the reported work of Poonam et al[19,20] for curved artery with aneurysm and stenosis, which is relevant in both studies. The comparison is done with Poonam et al[20] work for both the velocity and temperature in figures 2(a)-2(b). The hematocrit dependent viscosity parameter (h_m), Hartmann number (M), heat source or sink parameter $(\beta = 0)$ and thermal slip parameter $(\gamma = 0)$ have been neglected. Default values of the parameters have been utilized including $Gr = 0.8$, $Pr = 14$, $Re = 0.5$, $R_c = 3$, $Sb = 2.5$, $\sigma = 0.5$, $Pe = 1$, $B_1 = 1.41$, $B_2 = 0$, $\phi_1 = 0.05$, $\phi_2 = 0.05$.

Results and Discussion

The current mathematical work sought to investigate the effects of nanofluid hemodynamics and hematocrit-dependent viscosity on hemodynamics through a curved artery with stenosis and aneurysm. Hybrid nanoparticles, gold and copper, are used. The impact of many newly discovered characteristics, such as hematocrit number (h_m), Hartman number (M) on velocity profiles, radiation(Nr) on temperature and chemical reaction (ξ) on hybrid blood concentration profiles $(\phi_1 = \phi_2 = 0.05)$, is examined. Additionally, a comparison of these profiles for both the aneurysm and stenotic segments is done using MATLAB graphs.

In this present work Forward Time Central Space scheme is used to depict the graphs. The algorithms are created to calculate the velocity, temperature, concentration, microorganism impedance, Nusselt number (Nu), Sherwood number (Sh) Wall Shear-Stress (WSS) and volumetric flow rate (Q). The flow patterns for different physical parameters are studied. As listed in table 1, the default values of the parameters were used to complete the computational task. Table 2 demonstrates the thermophysical attributes of blood, gold and copper nanoparticles.

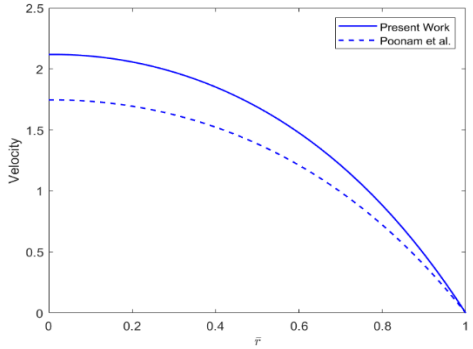

Fig. 2(a): Comparison of present study to published work for velocity.

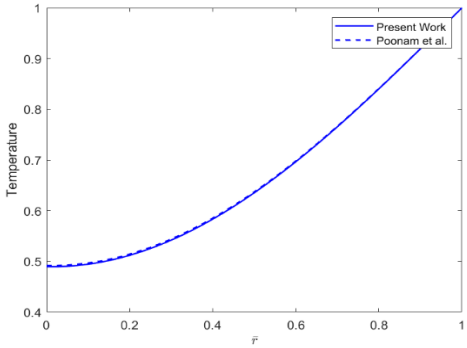

Fig. 2(b): Comparison of present study to published work for temperature.

Table 1
Values of physical attributes[9]

Physical property	Blood	Gold (Au)	Copper (Cu)
$c_p(J/kg\ K)$	3594	129	385
$\rho(kg\ m^{-3})$	1063	19320	8933
$\sigma\ (S\ m^{-1})$	6.67×10^{-1}	4.10×10^{7}	59.6×10^{6}
$k\ (W/m\ K)$	0.492	314	401
$\beta\ (K^{-1})$	0.18×10^{-5}	1.4×10^{-5}	1.67×10^{-5}

Table 2
Equations for the thermophysical parameters of nanofluids and hybrid nanofluids

Properties	Equations for the Thermophysical Parameters
Thermal Conductivity	$\frac{k_{nf}}{k_f} = \frac{k_{s1}+2k_f-2\phi_1(k_f-k_{s1})}{k_{s1}+k_f+\phi_1(k_f-k_{s1})}$, $\frac{k_{hnf}}{k_{nf}} = \frac{k_{s2}+2k_{nf}-2\phi_2(k_{nf}-k_{s2})}{k_{s2}+2k_{nf}+\phi_2(k_{nf}-k_{s2})}$
Electrical Conductivity	$\frac{\sigma_{nf}}{\sigma_f} = \frac{\sigma_{s1}+2\sigma_f-2\phi_1(\sigma_f-\sigma_{s1})}{\sigma_{s1}+2\sigma_f+\phi_1(\sigma_f-\sigma_{s1})}$, $\frac{\sigma_{hnf}}{\sigma_{nf}} = \frac{\sigma_{s2}+2\sigma_{nf}-2\phi_2(\sigma_{nf}-\sigma_{s2})}{\sigma_{s2}+2\sigma_{nf}+\phi_2(\sigma_{nf}-\sigma_{s2})}$
Viscosity	$\mu_{nf} = \frac{\mu_f}{(1-\phi_1)^{2.5}}$, $\mu_{hnf} = \frac{\mu_f}{(1-\phi_1)^{2.5}(1-\phi_2)^{2.5}}$
Heat Capacity	$(\rho C_p)_{nf} = \phi_1(\rho C_p)_{s1} + (1-\phi_1)(\rho C_p)_f$, $(\rho C_p)_{hnf} = [\phi_2(\rho C_p)_{s2} + (1-\phi_2)\{(1-\phi_1)(\rho C_p)_f + \phi_1(\rho C_p)_{s1}\}]$
Density	$\rho_{nf} = (1-\phi_1)\rho_f + \phi_1\rho_{s1}$, $\rho_{hnf} = \left[(1-\phi_2)\{(1-\phi_1)\rho_f + \phi_1\rho_{s1}\}\right] + \phi_2\rho_{s2}$
Thermal Expansion Coefficient	$\beta_f = (1-\phi_1)\beta_f + \phi_1\beta_{s1}$, $\beta_{hnf} = \left[(1-\phi_1)\{(1-\phi_1)\beta_f + \phi_1\beta_{s1}\}\right] + \phi_2\beta_{s2}$

Table 3
Numerical values of physical parameters

Parameters	Ranges
Hartmann Number (M)[1]	$0-4$
Schmidt Number (Sc)[29]	$0.5\ -\ 1.5$
Maximum Hematocrit (h_m)[20]	$0\ -\ 2$
Radiation Parameter (Nr)[20]	$0\ -\ 7$
Chemical Reaction Parameter (ξ)[20]	$0.5\ -\ 2$
Thermal Grashof Number (Gr)[4,23]	$0\ -\ 6$
Solute Grashof Number (Gm)[14]	$1\ -\ 6$
Prandtl Number (Pr)[14]	$14\ -\ 25$

Axial Velocity Profile: The influence of R_c (dimensionless radius of curvature of artery) on hybrid blood velocity is manifested in fig. 3. The dark lines epitomize the effect in the stenotic region and dashed lines shows effect in aneurysm region. These graphs show that increasing R_c for both stenosis and aneurysm segments causes the velocity profiles to rise**.** This happens due to reduction of centrifugal force acting on fluid. Although large amounts of R_c indicate a balanced distribution of velocity about center line. Additionally, it is noteworthy that due to constriction in stenosis region, there is narrowing in artery, so the hybrid-blood flow velocity in stenosis segment is found to be higher than aneurysm region's velocity at a certain value of R_c.

Fig. 4. illustrates how the Hartmann number M affects hybrid nanofluids' velocity. Standard values of Hartmann number are ranging from 0 to 4 as cited in table 3. In our investigation, we took values of $M = 1, M = 2,\ M = 3, M = 4$. Blood perceives a powerful electromotive force when subjected to an externally applied magnetic field. Due to hemoglobin, the magnetic field has a remarkable effect on the blood. Lorentz force causes a spike in blood viscosity, which diminishes flow velocity and may be favorable for controlling blood flow in artery. Increasing the magnetic intensity causes the blood velocity to drop. A velocity profile comparison between atherosclerosis and aneurysm demonstrates that for an identifiable magnetic parameter value, the hybrid blood' s velocity in aneurysm segment is higher than velocity in the stenotic segment.

The influence of thermal Grashof number (G_r) on hybrid blood velocity profile is demonstrated in fig. 5 for $G_r = 1, G_r = 2, G_r = 3.5, G_r = 5$. As cited in table 3, standard values of G_r are ranging from 0 to 6. The solid lines represent velocity profiles for stenotic region, while dashed lines correspond to aneurysm region.

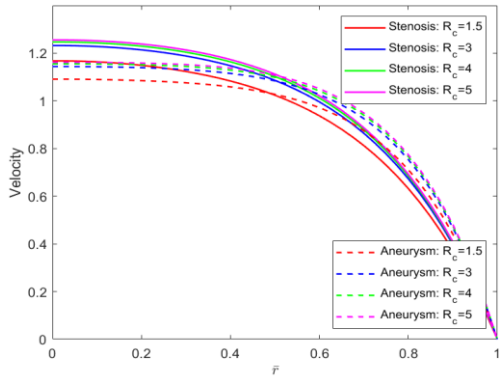

Fig. 3: Velocity variation with radius of curvature R_c

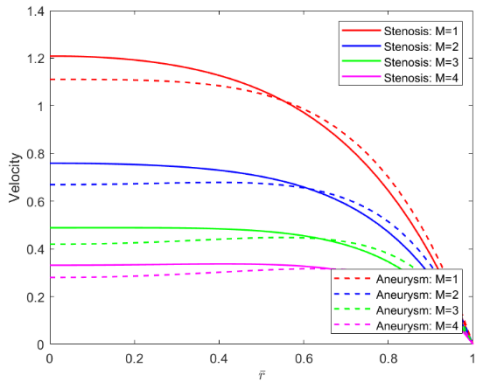

Fig. 4: Velocity variation with Hartmann Number M

In the context of natural convection, thermal Grashof number represents the ratio of the buoyant force acting on the fluid to its viscous force. It has been perceived that increased magnitude of (G_r) leads to the flow velocity to rise. This happens because fluid velocity rises when the viscous force surpasses the buoyant force in strength. For higher G_r i.e. $G_r = 5$, velocity profiles exhibit distinct behavior in stenotic and aneurysmal segments.

Velocity in the stenotic region is higher than aneurysmal segment at $G_r = 5$. This occurs due to the interplay of bouncy forces, constriction and recirculation effects. At this stage, the thermal buoyancy forces are stronger in stenotic region whereas in aneurysmal region, due to widening of artery, flow expansion come into role which leads to recirculation and energy dissipation that reduce the net velocity compared to stenosis region.

The impact of the solute's Grashof number (Gm) on hemodynamics velocity in the radial direction is observed in fig. 6. The typical values of Gm span from 1 to 6 as cited in table 3. Here in the figure 6, solid lines depict velocity profiles for stenotic region, while dashed lines represent velocity profile in aneurysm region. Graphical examination shows that when r changes from the center line to the artery wall, the flow velocity tends to zero.

The figure demonstrates that a higher value of Gm causes the viscous force to slow down, which in turn increases the flow velocity. As Gm increases, the buoyancy force become dominant that enhance natural convection leading to more significant velocity variations.

Temperature Profile: Fig. 7. illustrates how the Prandtl number alters the hybrid nanofluids' temperature in both the stenotic and aneurysm regions respectively. The standard values of Pr are ranging from 14 to 25 as cited in table 3. The ratio of momentum diffusivity to heat diffusivity is termed as the Prandtl number. The heat transfer from arterial wall to fluid (blood) is negatively correlated with Prandtl number. The temperature drops as the Prandtl number rises because thermal diffusion decreases. In comparison to the stenotic segment, the aneurysm segment has a lower temperature for the same value of Pr. It can also be said that as we move from the center line to the arterial wall, there is rise in the temperature.

For a range of radiation parameter (Nr) values, the temperature profile for hybrid nanofluid is epitomized in fig. 8. The temperature profile rises as Nr rises from 1.5 to 5, as the image illustrates. This transpires because thermal conductivity is impacted by the radiation parameter in the opposite manner, meaning that the system radiates the most heat. The blood uses radiation as an efficient heat source and as radiation dosage increases, the blood temperature rises. Although free electrons in gold and copper nanoparticles begin to oscillate when radiation of the proper wavelength interacts with them. It is also perceived that temperature in stenotic region is high compared to aneurysmal segment. This happens due to reason that higher shear stress and flow acceleration enhance thermal mixing, that leads to higher temperature in stenotic region. In contrast, aneurysm induces flow recirculation and vortex formation that result to reduce shear stress further lowering the temperature. Thermal treatment can greatly benefit from these findings.

Concentration Profile: The influence of chemical reaction parameter ξ on the concentration profile of hybrid blood in stenosis and aneurysm segments is displayed in fig. 9. As cited in table 3, typical values of chemical reaction parameter ξ span from 0.5 to 2. In our study we have taken values as $\xi = 0.5, \xi = 1, \xi = 1.5, \xi = 2$ and it is found that as the value of ξ rises, the figure shows that the hybrid blood's concentration falls. This occurs physically when the species concentration's chemical molecular diffusivity decreases as the chemical reaction parameter ξ increases. As a result, the species concentration lowers the fluid's overall mass transfer and has a retarding impact.

Micro-organism Profile: Fig. 10 epitomizes the microorganism variation due to bioconvective Lewis number Sb. The term "bioconvection" describes the fluid motion brought on by density gradients driven by collective activity of microorganisms. Here bioconvective Lewis-number Sb is taken to measures mass and heat diffusion processes in a particular system. It suggests that heat-

diffusion is dominant as compared to mass-diffusion by a greater bioconvective Lewis number. Conversely, mass diffusion is more significant than heat diffusion when the bioconvective Lewis number is lower. The flow reversal caused by the density difference among gyrotactic bacteria suppresses the concentration profile of microorganisms. Conversely, it is perceived from fig. 10 that density of motile organisms in blood decreases as the bioconvective Lewis number Sb rises.

It is also observed that an increase in bioconvection Lewies number enhances microorganism concentration in the artery, with stenosed region exhibiting higher microorganism concentration compared to aneurysmal region. Density of microorganism consistently decreases as parameter electrical conductivity (σ) rises, as shown in fig. 11. An increase in σ can account for the observed reduction by creating a larger density differential between gyrotactic microorganisms and fluid media around them.

The microorganisms' decreased diffusivity process is the cause of the density drop. As Sb and σ rise, the density of bacteria in the parent and daughter arteries falls. However the decline is more pronounced in stenosis region compared to anurysmal region suggesting that higher electrical conductivity surpasses microorganism accumulation more effectively in regions of stenosis.

Nusselt Number (Nu): Fig. 12 presents the variation of Nusselt number with respect for different values of Reynolds Number Re. Three distinct curves, corresponding to $Re = 0.5, 0.9, and\ 1.3.$, show the effect of increasing Reynolds Number on heat transfer. The Nusselt number exhibits a periodic oscillatory pattern, with higher Re values leading to an increase in overall magnitude of Nusselt number. The curves are vertically shifted, indicating different levels of convective heat transfer at each Re. As Re increases, thermal boundary layer is affected, modifying the heat transfer characteristics. This happens due to reason that higher Re implies a stronger convective transport, enhancing the heat transfer rate, which is reflected in Nusselt number. When Re increases, fluid motion intensifies, reducing the thermal boundary layer thickness and promoting more efficient heat dissipation. This leads to an increase in the absolute value of the Nusselt number, demonstrating enhanced convective heat transfer.

Sherwood Number Sh: Schmidt number Sc effect on Sherwood number can be detected by graphical representation from fig. 13 for stenosis and aneurysm section.

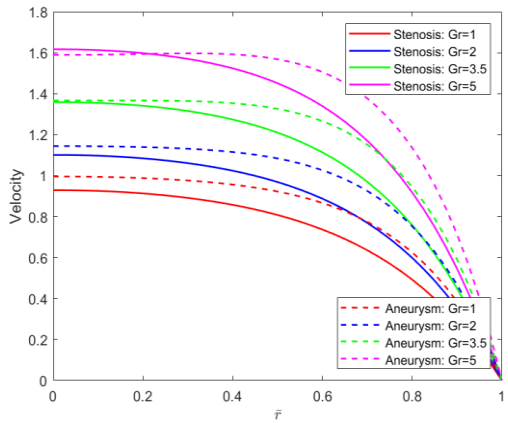

Fig. 5: Velocity variation with Grashof number (G_r)

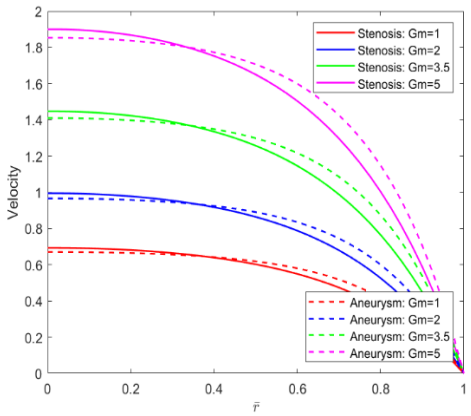

Fig. 6: Velocity variation with Grashof number (Gm)

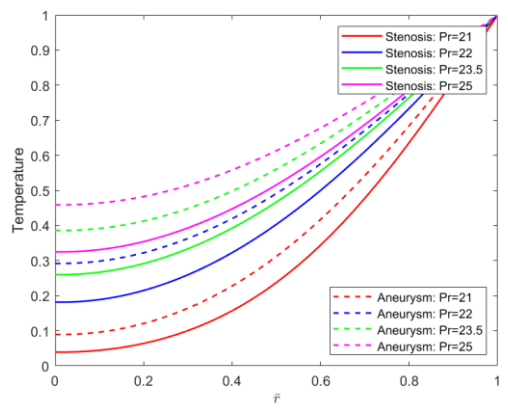

Fig. 7: Temperature variation with Prandtl number Pr

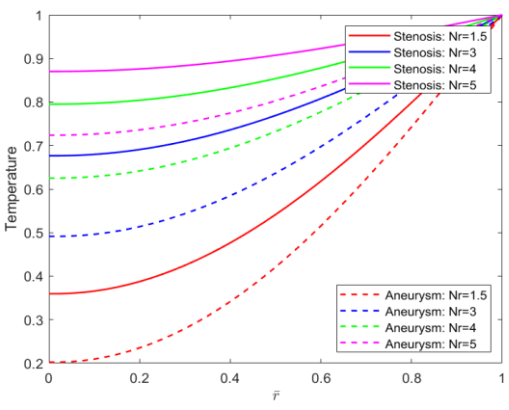

Fig. 8: Temperature variation with radiation parameter (Nr)

As cited in table 3, standard values of Schmidt number Sc are ranging from 0.5 to 1.5. As Sc increases, there is fall in the Sherwood number identified for both the segments atherosclerosis as well as aneurysm. This happens due to fact that as the Schmidt number Sc rises, mass diffusivity declines, resulting in weaker concentration gradients near the artery wall. This reduction in gradients lowers mass transfer, causing a decrease in the Sherwood number.

Wall Shear-Stress (WSS): The effect of magnetic field on wall shear-stress is depicted in fig. 14. Magnetic strength affects the wall shear-stress WSS due to the fact that magnetic field introduces a Lorentz force in the fluid, which acts against the flow. Magnetic field most affect near the wall of artery due to close reaction at wall as compared to center of artery. This force results to reduce velocity gradients close to the wall and hense increases WSS near the wall.

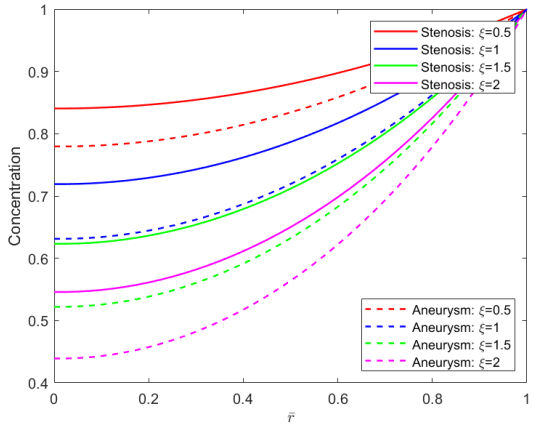

Fig. 9: Concentration variation with ξ in stenosis segment

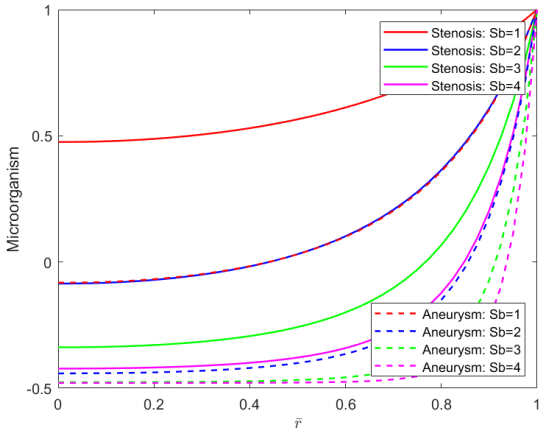

Fig. 10: Microorganism variation with bioconvective Lewis number Sb

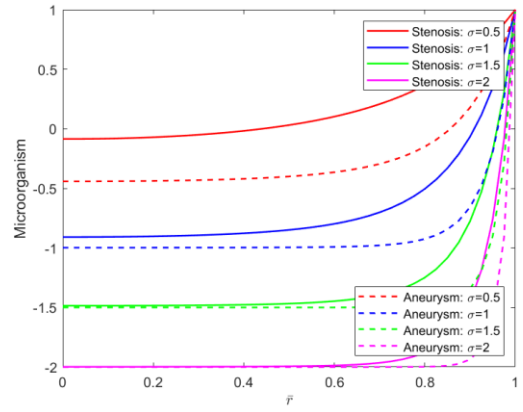

Fig. 11: Microorganism variation with electrical conductivity (σ)

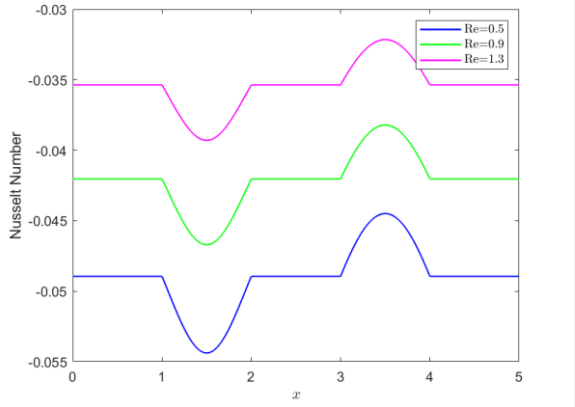

Fig. 12: Nusselt number variation with Reynolds Number Re

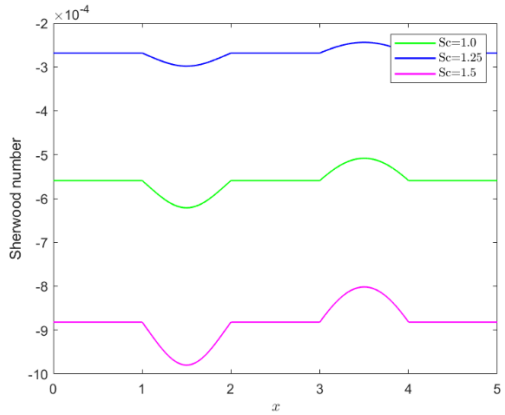

Fig. 13: Sherwood number variation with Schmidt number Sc

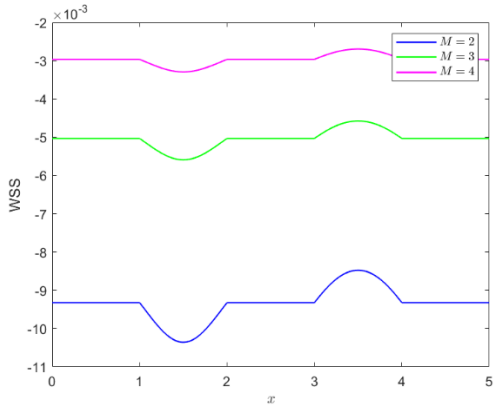

Fig. 14: Wall shear-stress variation with magnetic strength

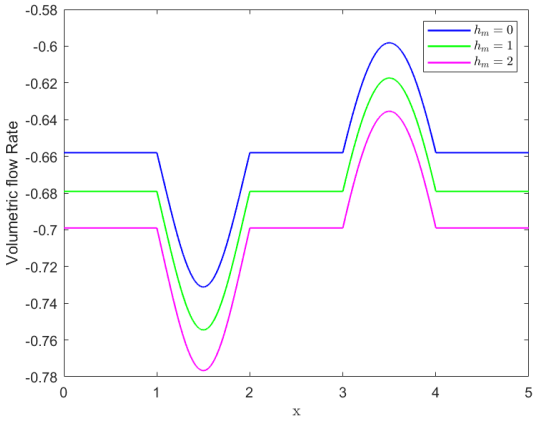

Fig. 15: Volumetric Flow rate variation with hematocrit perentage h_m.

Volumetric Flow Rate Q: The effect of hematocrit parameter h_m on volumetric flow rate of blood containing hybrid nanoparticles (Gold and Copper) is depicted in fig. 15. The graph illustrates how the flow rate varies along axial direction x for different values of $h_m = 0, h_m = 1, h_m = 2$. As h_m increases, the flow rate decreases in magnitude, indicating higher flow resistance. This happens due to the reason that higher h_m values correspond to enhance red blood cell aggregation along with stronger permeability effects, which introduce additional resistance to fluid motion and result in decrease in volumetric flow rate.

Conclusion

In the current manuscript, we investigated the behavior of blood flow in cardiovascular diseases such as stenosis as well aneurysm by adding hybrid nanoparticles gold and copper taking porous medium under the influence of varying magnetic field. This current study can be utilized to regulate the blood flow during biomedical treatments by adjusting the blood flow rate and heating effect due to the radiation by variation in strength of magnetic field, the concentration of nanoparticles, radiation and chemical reaction parameters. The key conclusions of our research are:

- That the flow velocity in both the stenosis and aneurysm region is relatively downstream as much the magnetic strength increases along the artery.
- As the bioconvective Lewis number (Sb) and electrical conductivity (σ) increases, there is a fall in microorganism interaction in arterial blood.
- The hybrid nanofluid containing gold and copper exhibits higher velocity compared to the hybrid nanofluid composed of gold and alumina.
- The reciprocal effect is noticed between the chemical reaction parameter (ξ) and concentration.
- Velocity increases for the rise in thermal Grashof number (Gr), solute Grashof number (Gm) and hematocrit percentage (hm). It is depicted that as Reynolds number (Re) increases, there is rise in heat transfer rate represented as Nusselt number (Nu).
- Temperature profile rises due to increment in radiation parameter (N_r) and Prandtl number (Pr).
- Sherwood number (Sh) and concentration profile diminish due to rise in Schmidt parameter (Sc) where Sherwood number represents mass transfer rate.
- Wall shear stress (WSS) rise as the magnetic field (M) increases over the artery. Volumetric flow rate (Q) decreases due to increase in hematocrit percentage (hm).

Acknowledgment

One of the authors, Sumit Sarowa is grateful for the financial support from University Grants Commission (UGC), New Delhi, India in the form of Junior Research Fellowship (JRF) (Award Number: 221610109498).

References

1. Abdel-wahed Mohamad S., Magnetohydrodynamic Ferro-Nano Fluid Flow in a Semi-Porous Curved Tube Under the Effect of Hall Current and Nonlinear Thermal Radiative, *J Magn Magn Mater*, **474**, 347-354, doi:https://doi.org/10.1016/j.jmmm.2018.11.050 **(2019)**

2. Alharbi F.M., Naeem M., Zubair M., Jawad M., Jan W.U. and Jan R., Bioconvection due to Gyrotactic Microorganisms in Couple Stress Hybrid Nanofluid Laminar Mixed Convection Incompressible Flow with Magnetic Nanoparticles and Chemical Reaction as Carrier for Targeted Drug Delivery Through Porous Stretching Sheet, *Molecules*, **26(13),** doi: 10.3390/ molecules26133954 **(2021)**

3. Anantha Kumar K., Sugunamma V. and Sandeep N., Effect of Thermal Radiation on MHD Casson Fluid Flow Over an Exponentially Stretching Curved Sheet, *J Therm Anal Calorim*, **140(5)**, 2377-2385, doi:10.1007/s10973-019-08977-0 **(2020)**

4. Bhargava R. and Chandra H., Numerical Simulation of MHD Boundary Layer Flow and Heat Transfer Over a Nonlinear Stretching Sheet in The Porous Medium with Viscous Dissipation Using Hybrid Approach, *arXiv*, http://arxiv.org/abs/1711.03579 **(2017)**

5. Changdar S. and De S., Analysis of Non-Linear Pulsatile Blood Flow in Artery Through a Generalized Multiple Stenosis, *Arabian Journal of Mathematics*, **5(1)**, 51-61 **(2016)**

6. Chung S. and Vafai K., Low-Density Lipoprotein Transport Within A Multi-Layered Arterial Wall—Effect of The

Atherosclerotic Plaque/Stenosis, *J Biomech*., **46(3)**, 574-585, doi: https://doi.org/10.1016/j.jbiomech.2012.09.022 **(2013)**

7. Gaidai O., Cao Y. and Loginov S., Global Cardiovascular Diseases Death Rate Prediction, *Curr Probl Cardiol*., **48(5)**, 101622, doi: https://doi.org/10.1016/j.cpcardiol.2023.101622 **(2023)**

8. Iasiello M., Vafai K., Andreozzi A. and Bianco N., Low-Density Lipoprotein Transport Through an Arterial Wall Under Hyperthermia And Hypertension Conditions – An Analytical Solution, *J Biomech*, **49(2)**, 193-204, doi: https://doi.org/10.1016/j.jbiomech.2015.12.015 **(2016)**

9. Imoro I., Etwire C.J. and Musah R., MHD Flow of Blood-Based Hybrid Nanofluid Through A Stenosed Artery With Thermal Radiation Effect, *Case Studies in Thermal Engineering*, **59**, doi: 10.1016/j.csite.2024.104418 **(2024)**

10. Kandasamy R., Periasamy K. and Prabhu K.K., Chemical Reaction, Heat And Mass Transfer On Mhd Flow Over A Vertical Stretching Surface With Heat Source And Thermal Stratification Effects, *Int J Heat Mass Transf*., **48**, 4557-4561, doi: 10.1016/j.ijheatmasstransfer.2005.05.006 **(2005)**

11. Kawaguti M. and Hamano A., Numerical Study on Post-Stenotic Dilatation, *Biorheology*, **20(5)**, 507–518, doi: 10.3233/BIR-1983-20508 **(1983)**

12. Kolin A., An Electromagnetic Flowmeter. Principle of The Method and Its Application to Blood Flow Measurements, Proceedings of the Society for Experimental Biology and Medicine, **35(1)**, 53-56, doi:10.3181/00379727-35-8854P **(1936)**

13. Kumar S. and Kumar S., MHD Two-layered Blood flow Under Effect of Heat and Mass Transfer in Stenosed Artery with Porous Medium, *International Journal of Advanced Research in Engineering and Technology (IJARET)*, **12(6)**, 63-76, doi:10.34218/IJARET.12.6.2021.007 **(2021)**

14. Kumawat C., Sharma B.K., Al-Mdallal Q.M. and Rahimi-Gorji M., Entropy Generation for MHD Two Phase Blood Flow Through a Curved Permeable Artery Having Variable Viscosity with Heat and Mass Transfer, *International Communications in Heat and Mass Transfer*, **133**, 105954, doi: https://doi.org/10.1016/j.icheatmasstransfer.2022.105954 **(2022)**

15. Mishra N., Computer Simulation of Heat and Mass Transfer Effects on Nanofluid Flow of Blood Through an Inclined Stenosed Artery with Hall Effect, *Acta Mechanica et Automatica*, **18**, 129-138, doi:10.2478/ama-2024-0017 **(2024)**

16. Moayeri M.S. and Zendehbudi G.R., Effects of Elastic Property of the Wall on Flow Characteristics Through Arterial Stenoses, *J Biomech*, **36(4)**, 525-535, doi: https://doi.org/10.1016/S0021-9290(02)00421-9 **(2003)**

17. Nadeem S. and Ijaz S., Theoretical Analysis of Metallic Nanoparticles on Blood Flow Through Stenosed Artery with Permeable Walls, *Phys Lett A*., **379(6)**, 542-554, doi: https://doi.org/10.1016/j.physleta.2014.12.013 **(2015)**

18. Pincombe B., Mazumdar J. and Hamilton-Craig I., Effects of Multiple Stenoses and Post-Stenotic Dilatation on Non-Newtonian Blood Flow in Small Arteries, *Med Biol Eng Comput*., **37(5)**, 595 – 599, doi:10.1007/BF02513353 **(1999)**

19. Poonam and Sharma B.K., Mathematical Analysis of Hybrid Nanoparticles on MHD Blood Flow Through a Curved Artery with Stenosis and Aneurysm Using Hematocrit-Dependent Viscosity, Springer Proceedings in Complexity, 978-3-030-99792-2 **(2022)**

20. Poonam, Sharma B.K., Kumawat C. and Vafai K., Computational Biomedical Simulations of Hybrid Nanoparticles (Au-Al2O3/ Blood-Mediated) Transport in a Stenosed and Aneurysmal Curved Artery with Heat and Mass Transfer: Hematocrit Dependent Viscosity Approach, *Chem Phys Lett*., **800**, doi: 10.1016/j.cplett.2022.139666 **(2022)**

21. Sharma B.K., Gandhi R., Mishra N.K. and Al-Mdallal Q.M., Entropy Generation Minimization of Higher-Order Endothermic/Exothermic Chemical Reaction with Activation Energy on MHD Mixed Convective Flow Over a Stretching Surface, *Sci Rep*., **12(1)**, 17688, doi: 10.1038/s41598-022-22521-5 **(2022)**

22. Sharma B.K., Khanduri U., Gandhi R. and Muhammad T., Entropy generation analysis of a ternary hybrid nanofluid (Au-CuO-GO/blood) containing gyrotactic microorganisms in bifurcated artery, *Int J Numer Methods Heat Fluid Flow*, **34(2)**, 980-1020, doi: 10.1108/HFF-07-2023-0439 **(2024)**

23. Sharma B.K., Kumawat C. and Makinde O.D., Hemodynamical Analysis of MHD Two Phase Blood Flow Through a Curved Permeable Artery Having Variable Viscosity with Heat and Mass Transfer, *Biomech Model Mechanobiol*, **21(3)**, 797-825, doi:10.1007/s10237-022-01561-w **(2022)**

24. Sharma B.K., Poonam and Chamkha A.J., Effects of Heat Transfer, Body Acceleration and Hybrid Nanoparticles (Au–Al2O3) on MHD Blood Flow Through A Curved Artery With Stenosis And Aneurysm Using Hematocrit-Dependent Viscosity, *Waves in Random and Complex Media*, doi: 10.1080/17455030.2022.2125597 **(2022)**

25. Shit G.C., Roy M. and Sinha A., Mathematical Modelling of Blood Flow through a Tapered Overlapping Stenosed Artery with Variable Viscosity, *Appl Bionics Biomech*, **11(4)**, 698750, doi: https://doi.org/10.3233/ABB-140102 **(2014)**

26. Yadav M., Yadav D., Kumar S. and Chhabra D., State of Art of Different Kinds of Fluid Flow Interactions with Piezo for Energy Harvesting Considering Experimental, Simulations and Mathematical Modeling, *Journal of Mathematical and Computational Science*, doi: 10.28919/jmcs/6772 **(2021)**

27. Sultan F., Alam Khan N., QaSim M. and Idrees Afridi M., Numerical Simulation of the Flow of Nano-Eyring-Powell Fluid through a Curved Artery with Time-Variant Stenosis and Aneurysm, *Nihon Reoroji Gakkaishi*, **47(2)**, 75-85 **(2019)**

28. Sultan F., Khan N., Khan M. and Afridi M., Numerical Simulation of the Flow of Nano-Eyring-Powell Fluid through a Curved Artery with Time-Variant Stenosis and Aneurysm, *Nihon Reoroji Gakkaishi*, 75-85, doi: 10.1678/rheology.47.75 **(2019)**

29. Kumar S. and Kumar S., Blood Flow through an Elliptical Stenosed Artery with Heat Source and Chemical Rection, *Res. J. Biotech.*, **17(12)**, doi: http://dx.doi.org/10.25303/1712rjbt82090, 82-90 **(2022)**

30. Tripathi B. and Sharma B.K., Influence of Heat and Mass Transfer on MHD Two-Phase Blood Flow with Radiation, In AIP Conference Proceedings, American Institute of Physics Inc., doi: 10.1063/1.5042179 **(2018)**

31. Tripathi B. and Sharma B.K., Effect of Variable Viscosity on MHD Inclined Arterial Blood Flow with Chemical Reaction, *International Journal of Applied Mechanics and Engineering*, **23(3)**, 767-785, doi:10.2478/ijame-2018-0042 **(2018)**

32. Wong K., Mazumdar J., Pincombe B., Worthley S.G., Sanders P. and Abbott D., Theoretical Modeling of Micro-Scale Biological Phenomena in Human Coronary Arteries, *Med Biol Eng Comput*., **44(11)**, 971-982, doi: 10.1007/s11517-006-0113-6 **(2006)**.

(Received 23rd April 2025, accepted 25th June 2025)